PERGAMON

International Journal of Heat and Mass Transfer 43 (2000) 849–866

International Journal of HEAT and MASS TRANSFER

www.elsevier.com/locate/ijhmt

Low turbulence natural convection in an air filled square cavity
Part I: the thermal and fluid flow fields

Y.S. Tian, T.G. Karayiannis*

School of Engineering System and Design, South Bank University, 103 Borough Road, London SE1 0AA, UK

Received 18 May 1998; received in revised form 4 June 1999

Abstract

An experimental study of low level turbulence natural convection in an air filled vertical square cavity was conducted. The dimensions of cavity were 0.75 m × 0.75 m × 1.5 m giving two-dimensional flow. The hot and cold walls of the cavity were isothermal at 50 and 10°C, respectively, giving a Rayleigh number of 1.58×10^9. The temperature and velocity distribution was systematically measured at different locations in the cavity, and was nearly anti-symmetrical. An experimentally obtained contour plot of the thermal field and a vector plot of the air flow in the cavity are reported for low turbulence natural convection in such cavities for the first time. The wall shear stress and the local and average Nusselt numbers are also presented. The Nusselt number compares well with previous results; the agreement on the velocity and temperature profiles at mid-height near the vertical walls is fair. Differences were found at mid-width and in the rate of velocity and temperature changes near the walls. The experiments were conducted with high accuracy. Therefore, the results can form experimental benchmark data and will be useful for CFD code validation.

Keywords: Natural convection; Cavity; Temperature distribution; Velocity; Heat transfer; Wall shear stress

1. Introduction

Natural convection in enclosures has been extensively studied experimentally and numerically. In numerical studies, natural convection in enclosures represents one of the simplest multiple-scale, coupled non-linear fluid flow problems and provides a convenient vehicle for the development of new analyses and new numerical algorithms. Among the various enclosures, the rectangular cavity is the most extensively studied enclosure because many engineering applications can be simplified to this geometry. These include solar collector cavities, air flow in rooms and other building structures such as cavity walls and double pane windows, cooling of electronic equipment, furnaces and others. Most of the early work concentrated on laminar flows and achieved considerable success. However, the study of turbulence natural convection still attracts the attention of researchers especially in the low level turbulence regime. Despite developments in the measurement techniques and instrumentation, as well as in the numerical methods and improved computing capability, the study of this low turbulence natural convection is still a challenge both in experimental and numerical terms. Advanced

* Corresponding author. Tel.: +44-171-815-7600; fax: +44-171-815-7699.

E-mail address: karayitg@sbu.ac.uk (T.G. Karayiannis).

0017-9310/00/$ - see front matter
PII: S0017-9310(99)00199-4

Nomenclature

a	parameter in Eq. (5)
Ar_x	aspect ratio $Ar_x = H/L$
Ar_z	aspect ratio in z-direction $Ar_z = D/L$
b	parameter in Eq. (5)
c	parameter in Eq. (5)
D	depth of the cavity (m)
d	diameter (m)
g	gravitational acceleration (m/s^2)
H	height of the cavity (m)
k	thermal conductivity (W/m K)
L	width of the cavity (m)
Nu	Nusselt number, $Nu = hL/k$
Pr	Prandtl number, $Pr = \nu/\alpha$
Ra	Rayleigh number, $Ra = g\beta(T_h - T_c)L^3/\alpha\nu$
Ra_H	Rayleigh number based on height, $Ra_H = g\beta(T_h - T_c)H^3/\alpha\nu$
S_p	stratification parameter, $S_p = \frac{L}{T_h - T_c}\frac{\partial T}{\partial y}$
T	temperature (K)
u^*	friction velocity, $u^* = \sqrt{\tau_w/\rho}$ (m/s)
u, v, w	velocity component (m/s)
V_0	the buoyancy velocity, $V_0 = \sqrt{g\beta\Delta TH}$ (m/s)
x_+	dimensionless distance from the wall
x, y, z	coordinate
X, Y, Z	dimensionless coordinate
α	thermal diffusivity (m^2/s)
β	thermal expansion coefficient (K^{-1})
μ	dynamic viscosity (kg/m s)
ν	kinematic viscosity (m^2/s)
ρ	fluid density (kg/m^3)
τ	shear stress (kg/m s^2)

Superscripts

-	time or integral average
′	fluctuation component
+	dimensionless parameter

Subscripts

b	bottom wall
c	cold wall
h	hot wall
i	component in i coordinate
t	top wall
w	wall
x	component along the width of the cavity
z	component along the depth of the cavity

experimental techniques have been used in the past but not without difficulty; accurate experimental work has been limited by the low absolute velocity values and the fact that the fluid flow and heat transfer inside a rectangular cavity are very sensitive to the experimental and boundary conditions. In numerical studies, the strong coupling of the boundary layer and the core flow makes computation very difficult. Direct simulation of turbulent natural convection in a cavity is still too costly. Numerical results from various k–ε models are non-unique. In addition, none of the turbulence models can correctly predict whole velocity and temperature fields.

A significant number of experimental and theoretical works had been carried out in the past decade in an attempt to understand turbulent flow in enclosures. Catton [1], Hoogendoorn [2], Ostrach [3] and Yang [4,5] gave very good reviews, covering the earlier work in this area. In the 1992 Eurotherm Seminar 11 [6], many researchers made their contributions for the standard case ($Ra = 5 \times 10^{10}$, $Ar_x = 1$ with adiabatic horizontal walls). The agreement between the contributions was particularly good for quantities in the inner layer (from the wall to the velocity maximum), e.g., at the cavity mid-height, half of the results giving the wall heat transfer, and the vertical velocity maximum differ by less than 5% and 1%, respectively. However, differences in the reported turbulent quantities were significant. The numerical results for the standard case were not confirmed by any experimental results because the assumed adiabatic boundary conditions on the horizontal walls are extremely difficult to realise in air filled enclosures. Up to now, experimental data for turbulent natural convection are still scarce, especially for the square cavity as most of the experiments were conducted with high or tall cavities. On the other hand, most of the numerical modelling results were obtained for square cavities.

In general terms, the study of turbulent natural convection in cavities is still at an early stage. Correlations from both experimental and numerical studies are available for the prediction of heat transfer across the cavity. However, a comparison between experimental and numerical velocity and temperature profiles reveals discrepancies. Also, as mentioned above, the experimental results are mostly for non-ideal boundary conditions and the numerical results are not free from the non-unique solutions. Further, the study of turbulent fluctuation quantities is at its infancy. Therefore, carefully designed experiments are needed to provide benchmark data and this has been the objective of the work presented in this paper and [7].

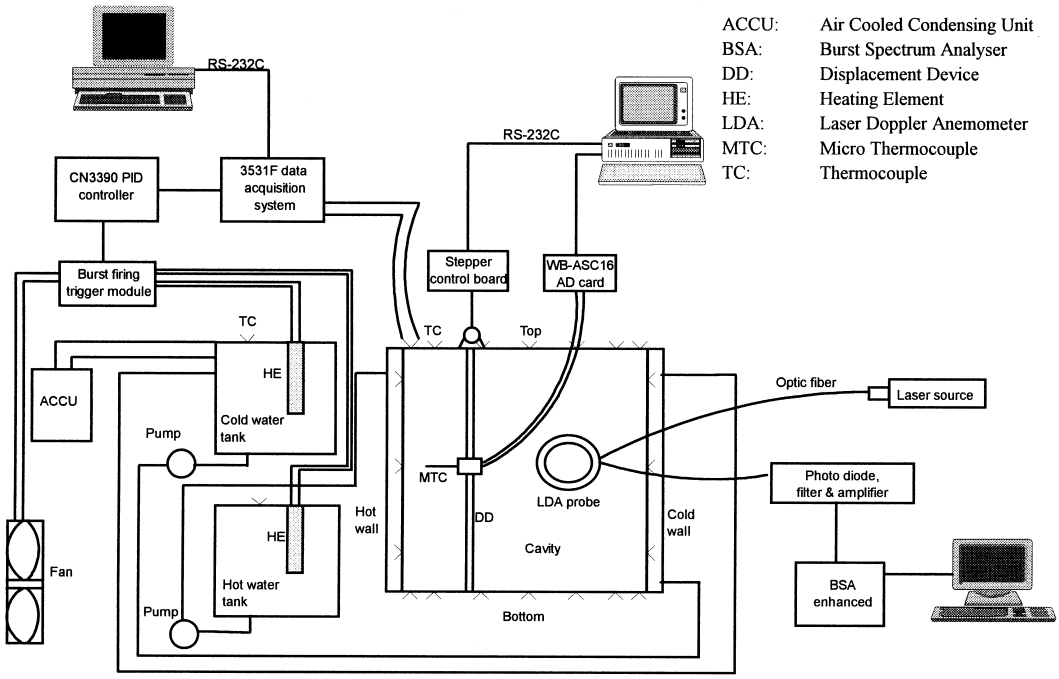

Fig. 1. Schematic diagram of the experimental facility.

2. Experimental facility and procedure

A fully automatically controlled natural convection test rig has been carefully designed and constructed. The experimental facility, which is shown in Fig. 1, can be divided into four parts: the temperature control system, the cavity, and the facilities for measuring the air temperature and velocity. The temperature control system maintained a constant temperature water flow to two chambers attached to the hot and cold plates,

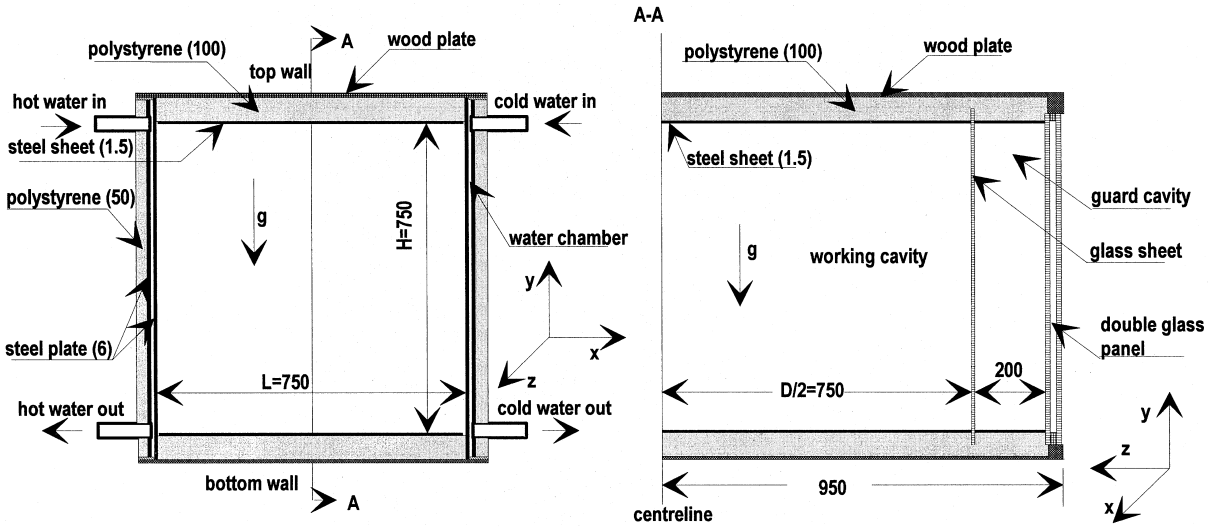

Fig. 2. Schematic of the air filled square cavity (all dimensions are in mm and the axis origin is at the bottom of the hot wall and the cavity centre line).

see Fig. 2. It comprised a PC, a Schlumberger 3531F data acquisition system, a multi-loop PID (proportional-integral-differential) temperature-process controller and low noise K-type thermocouples. The computer controlled the data logging system to record the thermocouple readings and to send the signal to the PID controller. The PID controller sent pulses to the burst firing trigger modules to alter the heating power. The burst firing trigger modules switched the power on and off at zero voltage. Therefore, the whole system was free from radio frequency noises. The ambient, the cold water and the hot water were controlled at a predetermined temperature. The cold and hot water were pumped through the water chambers at a rate of 40 L/min. The dimensions of test cavity, shown in Fig. 2, were 0.75 m × 0.75 m × 1.5 m. With two guard cavities on each side, this air filled cavity offers two- dimensional flow in the middle. Temperatures on the isothermal and the horizontal walls were measured using K-type thermocouples. There were in all 62 pairs of thermocouples, 12 on each of the isothermal walls and 19 on each of the horizontal walls. The thermocouples and data logging devices were calibrated using National Physical Laboratory thermometers (with 0.02 K accuracy) and an oil bath. The hot and cold walls of the cavity were made of 6 mm mild steel plate and maintained isothermal at 50 ± 0.15 and 10 ± 0.15°C, respectively giving an Ra of 1.58×10^9. The top and bottom walls were made from 1.5 mm mild steel sheet and provided highly conducting boundaries. The room temperature was controlled at 30 ± 0.2°C, chosen to be equal to the cavity average temperature (average of the hot and cold wall temperatures). The guard cavities and the well controlled ambient temperature resulted in maintaining the heat and mass transfer across the cavity walls to a minimum. An E-type thermocouple of diameter 25.4 μm was carried by a computer controlled two-dimensional displacement device and was used to measure the air temperature in the cavity. The temperature was read by a 16 bit data logging card at 50 Hz sample rate. For every location, 4096 readings were taken. The average and fluctuation temperatures were recorded. The displacement device was calibrated using a dial indicator (with 0.01 mm positional accuracy). The accuracy of the thermocouple location was better than 0.2 mm and the temperature reading was true within 0.1 K. A back scatter, 2D Laser Doppler Anemometer (LDA) with a Burst Spectrum Analyser (BSA) and a 40 MHz frequency shift Bragg cell was used in the velocity measurements. The laser source was a 300 mW argon laser. The measured velocity range was from −0.5082 to +0.5082 m/s with a resolution of 6.20E−5 m/s at a bandwidth of 0.125 MHz. The laser beams entered the cavity through the guard cavity with a 3.5 angle to the isothermal wall. A front

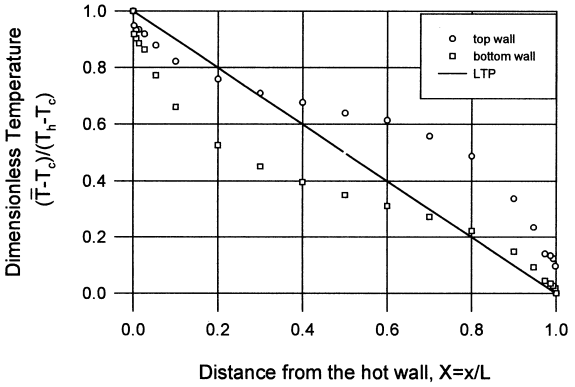

Fig. 3. Temperature distribution along the horizontal walls.

lens with a focal length of 1200 mm was used. The probe volume dimensions were 0.31 mm (diameter) × 9.8 mm (length). Incense smoke was used as seeding which lasted for more than 24 h. For every measuring point, either 20 K readings were taken or the measurement period was 4 min. The velocity was extensively surveyed near the walls. The 3D traverse mechanism which carried the LDA probe was calibrated using a dial indicator (with 0.01 mm accuracy). The accuracy of the laser location was better than 0.1 mm. The resulting uncertainty in the processed data was very small. The error in the Ra was 1.515×10^6 or 0.6%. The error in the Nu was 0.2133 and in the wall stress 1.5%. Further details of the experimental facility, procedure and uncertainty analysis are available in Ref. [8].

The temperature distribution was measured at the cavity mid-plane ($Z = 0$) on a very fine non-uniform mesh. First, the temperature was measured at 19 different heights and for each height at 101 points from the hot wall to the cold wall. The temperature changed sharply near the isothermal walls. Therefore, at the first 3 mm from the wall, the temperature was measured at every 0.25 mm. From 3 to 10 mm from the wall, the temperature was measured at every 0.5 mm. From 10 mm to the cavity centre, the distance between consecutive measuring points was increased from 1 to 37.5 mm. Subsequently, the temperature near the horizontal walls was intensively measured. The velocity distribution was measured on the same mesh. The LDA probe could be positioned to the wall with a small angle so that the measuring point reached all the positions in the cavity. During all the measurements, the experimental conditions were kept as steady as possible. Experimental repeatability was verified. The maximum deviation between readings obtained during experiments performed at different times was 0.5 K for the temperature and 2 mm/s for the velocity.

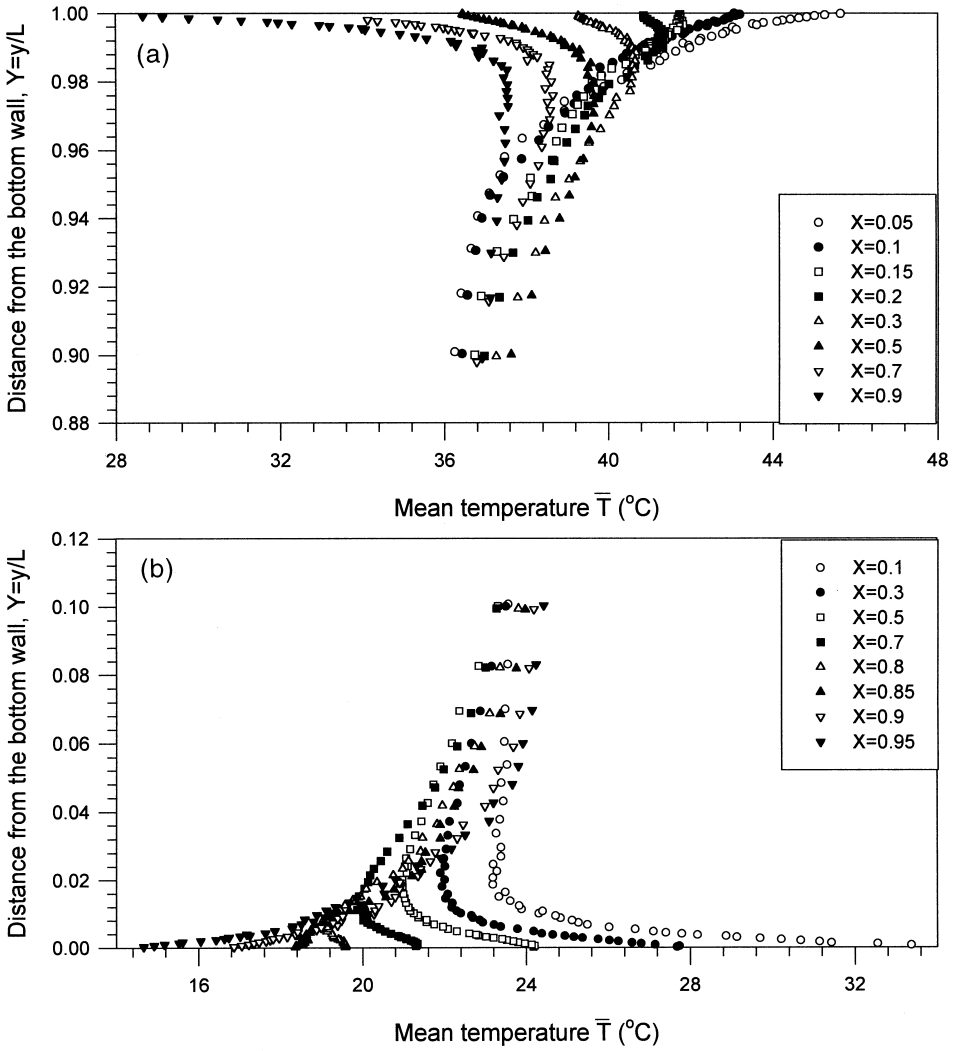

Fig. 4. Temperature distribution near the horizontal top and bottom walls: (a) the top wall; (b) the bottom wall.

3. Experimental results

3.1. The temperature distribution

As mentioned above, the two isothermal walls were kept at 50 and 10°C at all times while the horizontal walls were built to be highly conducting. A typical temperature distribution on the horizontal walls is shown in Fig. 3 and compared with the ideal linear temperature distribution (LTP). This temperature distribution, representing real boundary conditions, is recommended for numerical modelling. The temperature distribution near the top and bottom walls is shown in Fig. 4. A total of 27 locations were measured, but only eight are shown in the figure for clarity [8]. The temperature changes abruptly from the wall to $Y = 0.02$ on the bottom and $Y = 0.98$ on the top. Along the walls, the temperature profiles changed because the heat flux changed direction at about $X = 0.175$ on the top wall and $X = 0.825$ on the bottom wall. This is discussed later when the local Nu number results are presented. Between $X = 0.05$ and 0.15 on the top wall, the temperature decreases monotonously from the wall to $Y = 0.9$. Between $X = 0.20$ and 0.9, the temperature first increases sharply from the wall to a maximum around $Y = 0.98$ and then decreases slightly to about 36.5°C around $Y = 0.9$. The temperature distribution near the bottom wall is anti-symmetrical with that near the top wall.

The temperature distribution for different heights is depicted in Fig. 5. The temperature of the core was 30.75°C which is nearly equal to the mean temperature

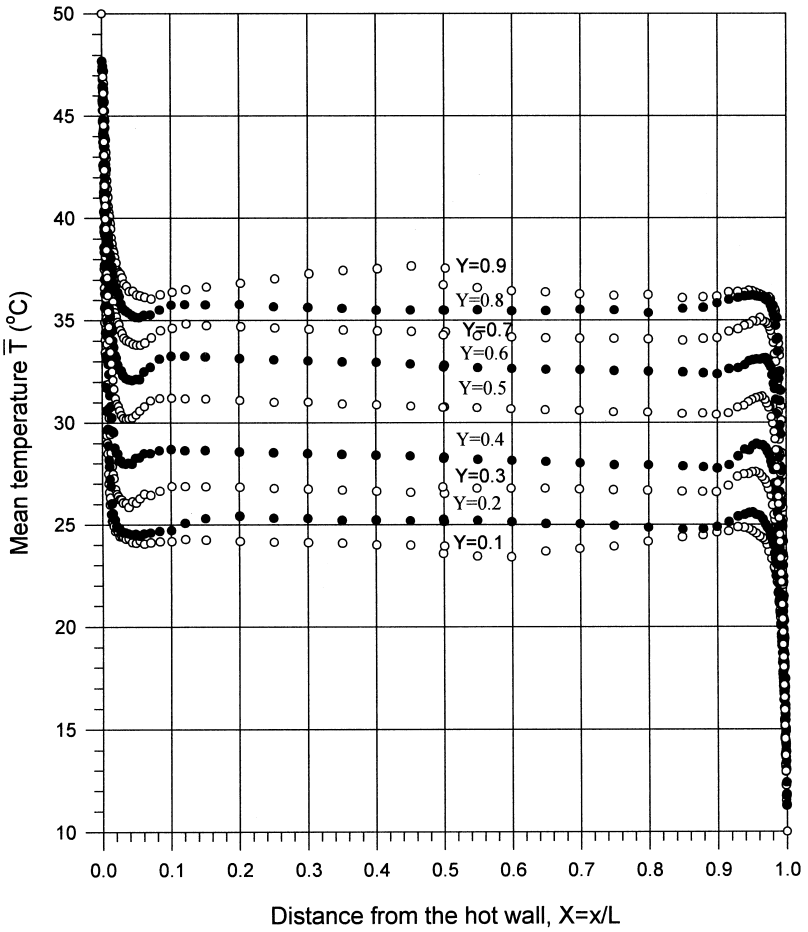

Fig. 5. Temperature distribution at different heights.

(and the ambient), indicating that no heat is lost through the passive vertical walls, i.e., through the guard cavities. The dimensionless temperature at the cavity centre was 0.514. It can be seen in the figure that the temperature distribution is nearly anti-symmetric about the cavity centre. Across the cavity, in the horizontal direction, the temperature has a steep change near the two isothermal walls, which was limited in a very narrow strip ($\Delta X = 0.05$ from the wall). From $X = 0.1$ to 0.9, the temperature decreased only slightly, indicating that the fluid in the core area was nearly stationary. The temperature over-shoot was obvious around $X = 0.035$ and 0.965. The temperature distribution in the area $X = 0.1$–0.9, $Y = 0.1$–0.9 shows stratification. A contour plot of the thermal field is shown in Fig. 6. This is based on all the experimental data. However, due to the limitation of the PC and software, the data were inserted into a 38×38 non-uniform mesh which was coarser than the measurement mesh. This accounts for some lack of smoothness in the contour plots. In a cavity with adiabatic horizontal walls the stratification of the core extends closer to the walls than in a cavity with LTP boundary conditions. In our case, the extend of the stratified region reflects the fact that the walls are highly conductive, i.e., this region is larger than the adiabatic case and smaller than the LTP case. In the figure, there are two peaks near the isothermal walls, one near the hot wall and other near the cold wall. The distance from wall to the peak point is increasing along the flow direction, i.e., the thickness of the inner layer of the thermal boundary is increasing along the flow direction. The thickness of the thermal boundary is thicker than a cavity with adiabatic horizontal walls and is thinner than a cavity with perfect conducting walls [9].

3.2. The velocity distribution

The measured vertical and horizontal velocity components at different heights are shown in Fig. 7(a) and (b), respectively. In the figure, a constant was added to

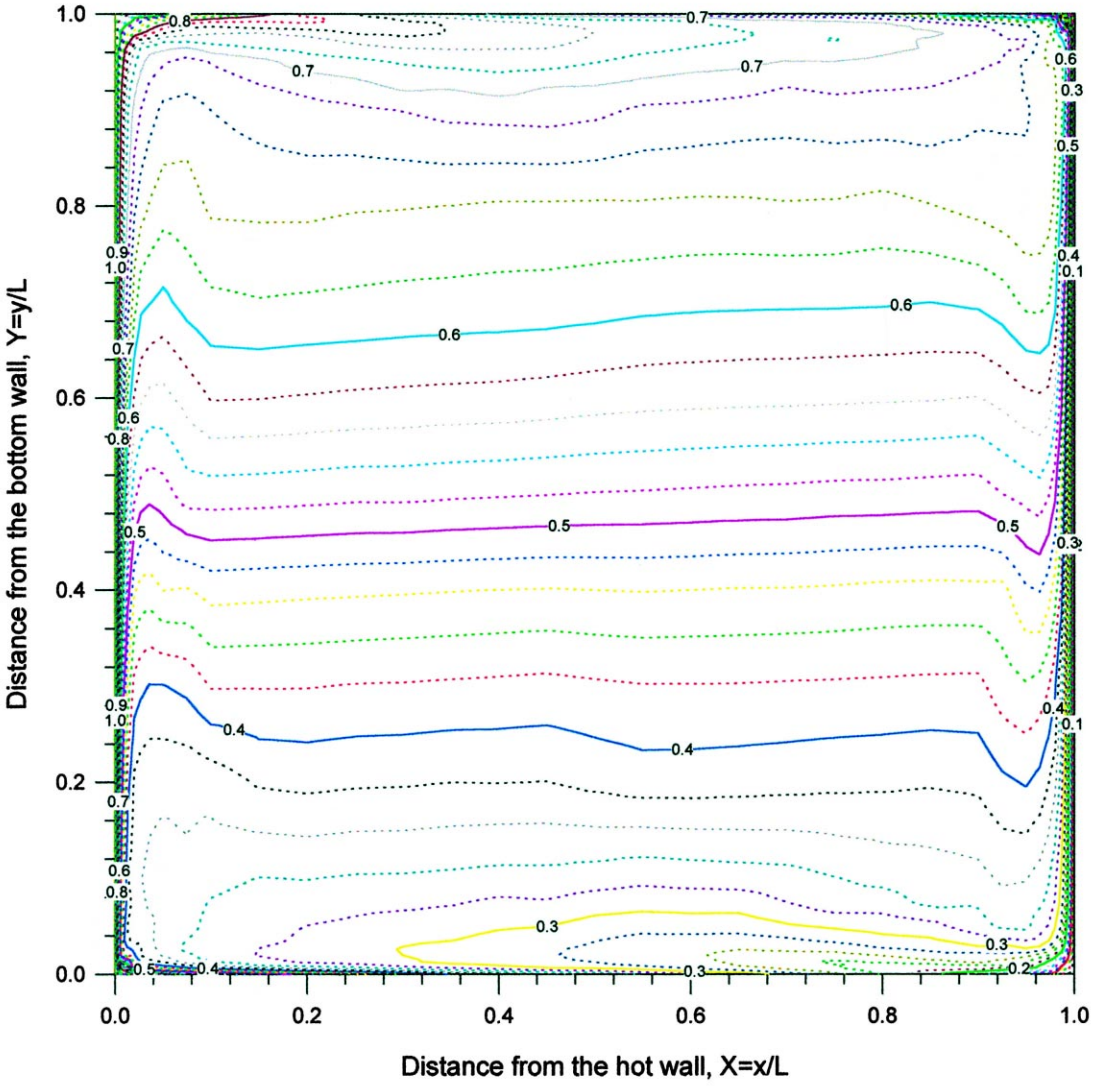

Fig. 6. Contour plot of temperature distribution, $(\bar{T} - T_c)/(T_h - T_c)$, in the cavity.

the value of the velocity at different heights to avoid data overlap. V_0 is the buoyancy velocity defined as $V_0 = \sqrt{g\beta H\Delta T}$ and in our case is equal to 1 m/s. In general, the horizontal velocity component is one order of magnitude smaller than the vertical component and its distribution changes significantly at different heights. The flow boundary layer along the isothermal walls can be seen clearly from the vertical velocity distribution at different heights. The boundary layers start at the bottom of the hot wall and at the top of the cold wall with a small peak velocity and large thickness. The boundary layer becomes thinner along the flow direction and the peak velocity increases. The boundary layer reached minimum thickness at about $Y = 0.4$ at the hot wall and $Y = 0.6$ at the cold wall. The velocity peak reaches its maximum value (0.225 m/s) at this location. After this point, the layer gets thicker in the direction of flow with the peak velocity decreasing. The whole fluid flow vector plot in the cavity is given in Fig. 8. As was the case with the temperature plot, the velocity vector plot is based on all the experimental data but is plotted on a mesh which is more coarse than the measurement mesh. A sketch in Fig. 9 shows the flow structure in the cavity. It consists of boundary layer flow along all cavity walls with two small vortices at the top-hot and bottom-cold corners. These vortices are about $d/L = 0.01$ in diameter and of anti-clockwise rotation. To the best of the authors' knowledge, the existence of the small vortices in a vertical cavity has not been reported previously.

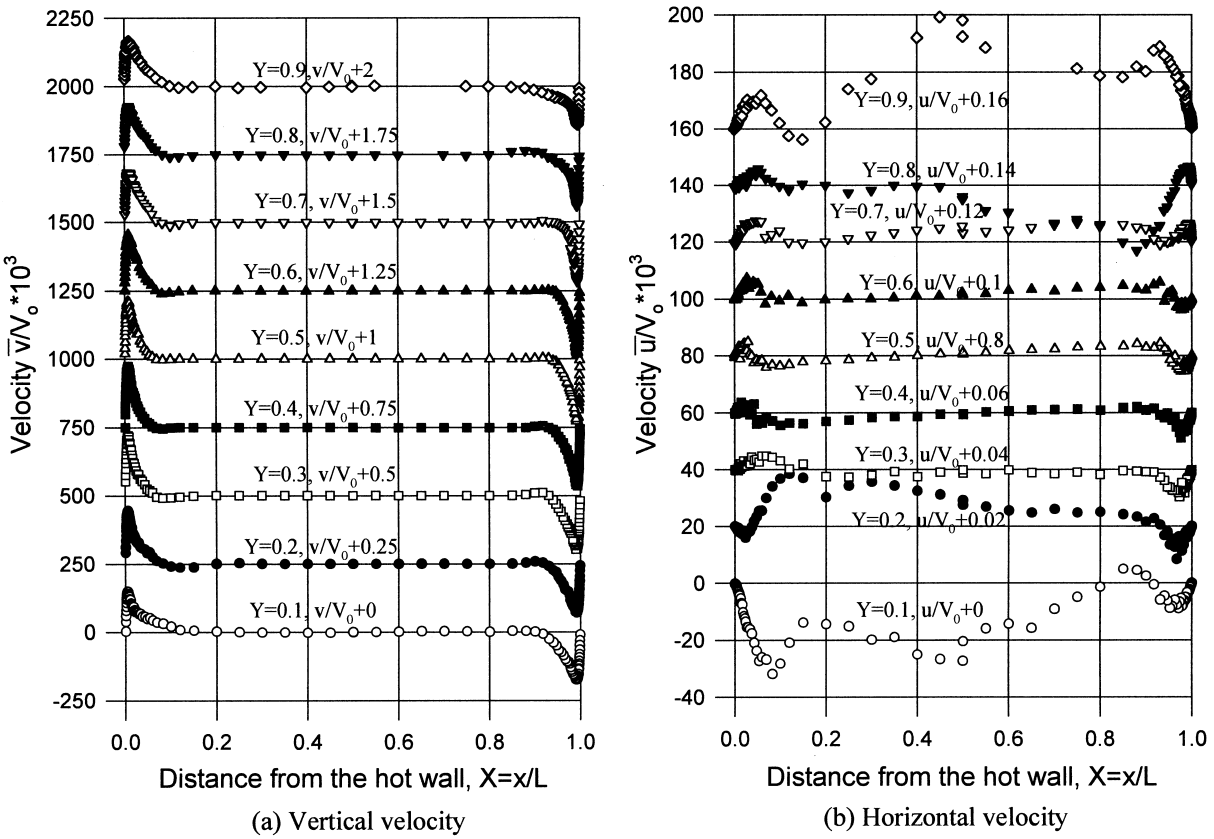

Fig. 7. Mean velocity distribution at different heights: (a) vertical velocity; (b) horizontal velocity.

Examination of the vertical velocity profiles of Fig. 7 shows small negative velocity values indicating circulatory clockwise motion outside the vertical boundary layers for $0.075 < Y < 0.925$. Similar vortex motion exists at the outer edge of the horizontal boundary layers as indicated by the vector plot of Fig. 8(a) and shown in Fig. 9. The boundary forming process as seen clearly in Figs. 7 and 8 is different from the boundary layer that forms over a flat plate. For forced flow over a plate, the boundary layer forms at the starting point of the plate. In the boundary layer, the fluid is dragged by the wall to reduce its speed while part of the fluid is pushed out of the boundary layer. For free convection over an isothermal plate, the fluid in the boundary layer is taken from the stationary ambient. The size of the ambient is large as compared to the thickness of the boundary layer so that there is no flow reversal. In natural convection in a square cavity, the vertical boundary layer inherits mainly from the horizontal boundary layer especially at the starting corners, see Figs. 8 and 9. Some of the ambient fluid is involved in the flow as the boundary layer develops. The limited size of the ambient causes flow reversal and the rotational motion at the outer edges of the boundary layers, seen in Fig. 9.

4. Discussion and comparison

Before we discuss and compare the present results with earlier studies, the assumption of 2D flow should be clarified. In a numerical solution, 2D modelling assumes that the length in the third direction is long enough so that its influence can be neglected. However, in experiments this is not easily achieved. Up to now, most of the experimental studies were assumed 2D even though the experimental cavity dimensions were such that 3D flow prevailed. How deep a cavity should be for a 2D or even a quasi-2D thermal and fluid flow pattern? Penot and N'Dame [10] pointed out that the 2D approximation of experimental natural convection in cavities should be valid if the horizontal aspect ratio (Ar_z) of the cavity is greater than 1.8. The experimental studies of Lankhorst [11], Mergui and co-workers [12,13] and Opstelten et al. [14] did not satisfy this requirement

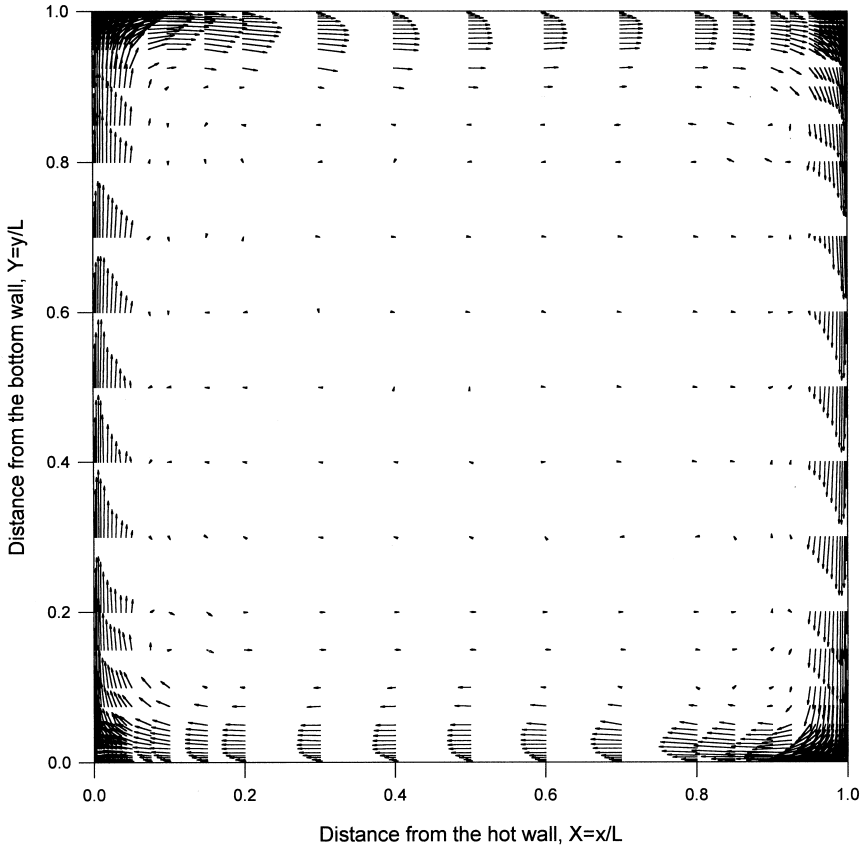

(a) the whole cavity (Scale: 0.02 m/s /mm)

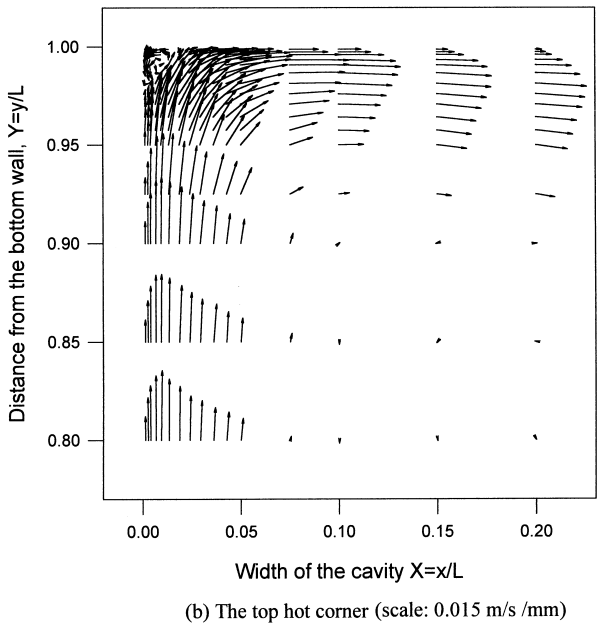

(b) The top hot corner (scale: 0.015 m/s /mm)

Fig. 8. (a) The whole cavity (scale: 0.02 m/s mm^{-1}); (b) the top hot corner (scale: 0.015 m/s mm^{-1}).

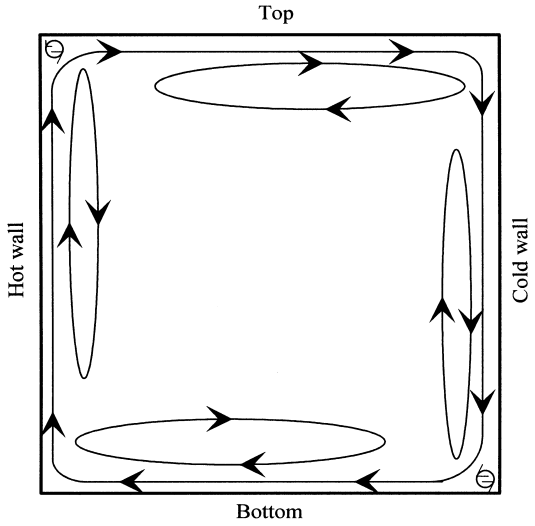

Fig. 9. Sketch of the flow structure in the cavity.

and hence their results were affected by the small cavity depth. Further, even if the depth is large, the heat loss through the passive vertical walls and the ceiling can still cause the 3D flow [15,16]. Because of this heat loss, fluid flow in the cavity bears the features of stronger asymmetry, higher turbulence and lower average temperature at the cavity centre. In this study, the aspect ratio in the depth direction is 2. As mentioned in Section 2, two guard cavities were connected to the vertical passive walls on each side. The ambient temperature was set to be the same as the average temperature of the hot and cold wall and the cavity was insulated. Hence the heat and mass transfer across the cavity walls was reduced to a minimum. The two dimensionality of the flow was verified by comparing the velocity distribution at three different cavity depths, $Z = 0$, 0.533 and 0.8, see Fig. 10. The three profiles differ only by 4% on the peak velocity and 0.5 mm on its position, which indicates that the depth of the cavity, the guard cavities and the ambient of 30°C provided a 2D field. Very near the side walls ($Z \approx \pm 1$) some 3D can be expected but this did not affect the flow and thermal fields at the cavity centre.

As designed, the flow in the present cavity is in the low turbulence flow region, i.e., a turbulent wall shear flow. As shown in Figs. 8 and 9, the flow was limited in the boundary layers along the walls and the flow does not reach the fully developed region, i.e., the velocity profile changes along the flow direction. A natural turbulent boundary layer can be described in a two layer structure, namely an inner layer and an outer layer [17], separated by the position of the velocity

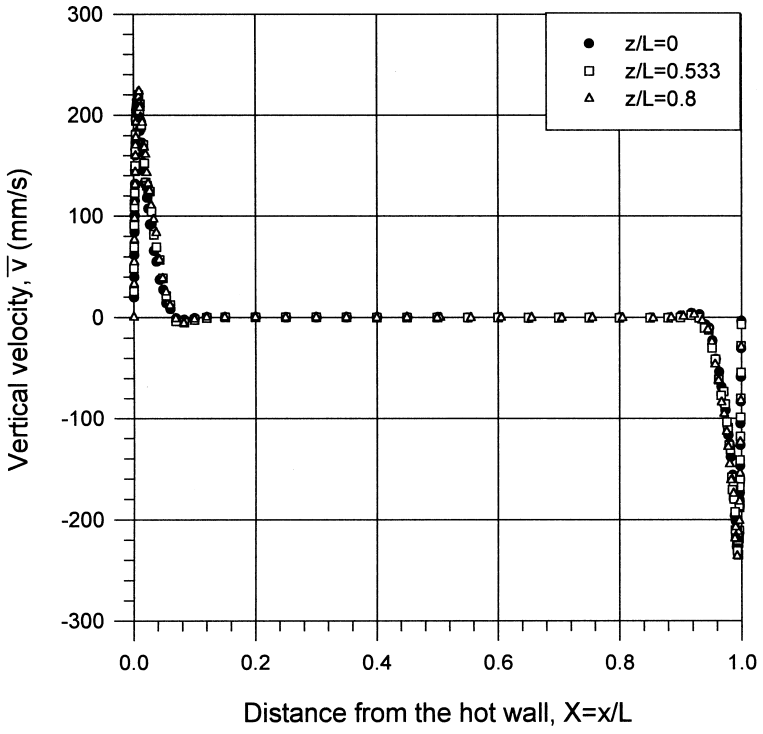

Fig. 10. Comparison of the mean velocity at $Y = 0.5$ and $Z = 0$, 0.533 and 0.8.

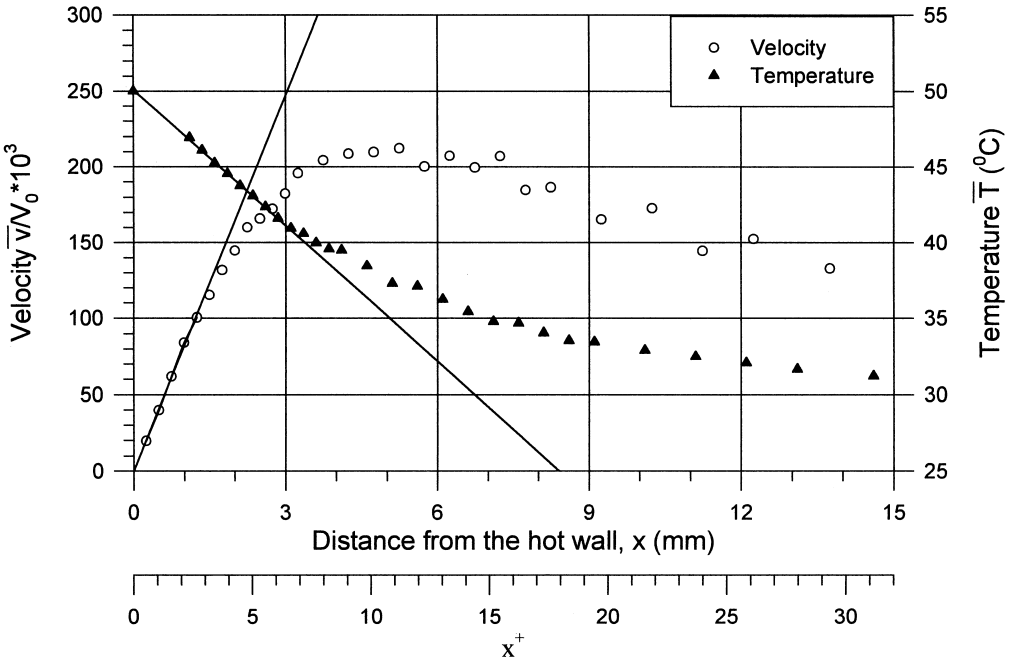

Fig. 11. Mean vertical velocity and temperature near the hot wall at $Y = 0.5$.

maximum. The inner layer can be divided further in a viscous layer next to the wall where the Reynolds stress is negligible (see Ref. [7]) and buoyant sub-layer in the rest of the inner layer. In the viscous layer, very close to the wall, the temperature profile is nearly linear, see Fig. 11. This is referred to as conductive layer in which the heat flux is constant [18]. Within this layer, the velocity profile is cubic in distance from the wall. The velocity profile in the buoyant and outer layer is different from the forced turbulent wall flow, where the velocity profile is logarithmic in the outer layer. In the present case, the velocity reaches its maximum between the buoyant layer and the outer layer and drops to a negative peak in the outer layer due to the reverse flow. In the two equation standard k–ε model numerical simulations, the wall function, i.e., the logarithmic velocity profile near a solid wall, is helpful since it saves many grid points. However, the logarithmic velocity profile does not exist in this low turbulence natural convection in a square cavity.

The measured results in the boundary layer can be used to determine two integral parameters, Nusselt number and wall shear stress. The Nu number along the walls can be determined using the measured temperature in the thermal conductive layer where the heat flux is constant. The local Nu number is defined as:

$$Nu = -\frac{L}{T_h - T_c}\frac{\partial T}{\partial x_i}\bigg|_w \tag{1}$$

From the definition, the heat flux is positive with axis direction, i.e. heat transfer from the hot wall into the cavity and from the cavity into the cold wall is positive. Heat transfer from the bottom wall into the cavity and from the cavity into the top wall is also positive. The temperature gradient with respect to x and y was estimated by linear best fit using the first 5–9 measuring locations near the wall. The local Nu on the hot and cold walls of the cavity is shown in Fig. 12(a). It reaches its maximum at the bottom of the hot wall and at the top of the cold wall because of the thinner thermal boundary layer there. The measured maximum Nu value is about 135. As the thickness of the boundary layer increases along the flow direction, the local Nu decreases rapidly and is about 58 at mid-height. At the other end, the heat transfer diminishes significantly when the fluid flow meets the wall and the local Nu drops to 17. The average Nu was 64 and 65.3 for the hot and cold walls, respectively. The difference for the two sides is less than 2%. Fig. 12(b) depicts the local heat transfer along the top and bottom walls. One noticeable feature is the change in the direction of heat flux, i.e., on one part of the horizontal wall, heat is transferred from the wall into the cavity and on the remaining part, heat is transferred from the cavity into the wall. The change occurred at $x/L \approx 0.175$ and 0.825 at the top and the bottom, respectively. At the bottom wall, heat is transferred from the wall to the air at $X = 0$–0.825 and from the air to the wall at $X = 0.825$–1; at the top wall, heat is transferred from

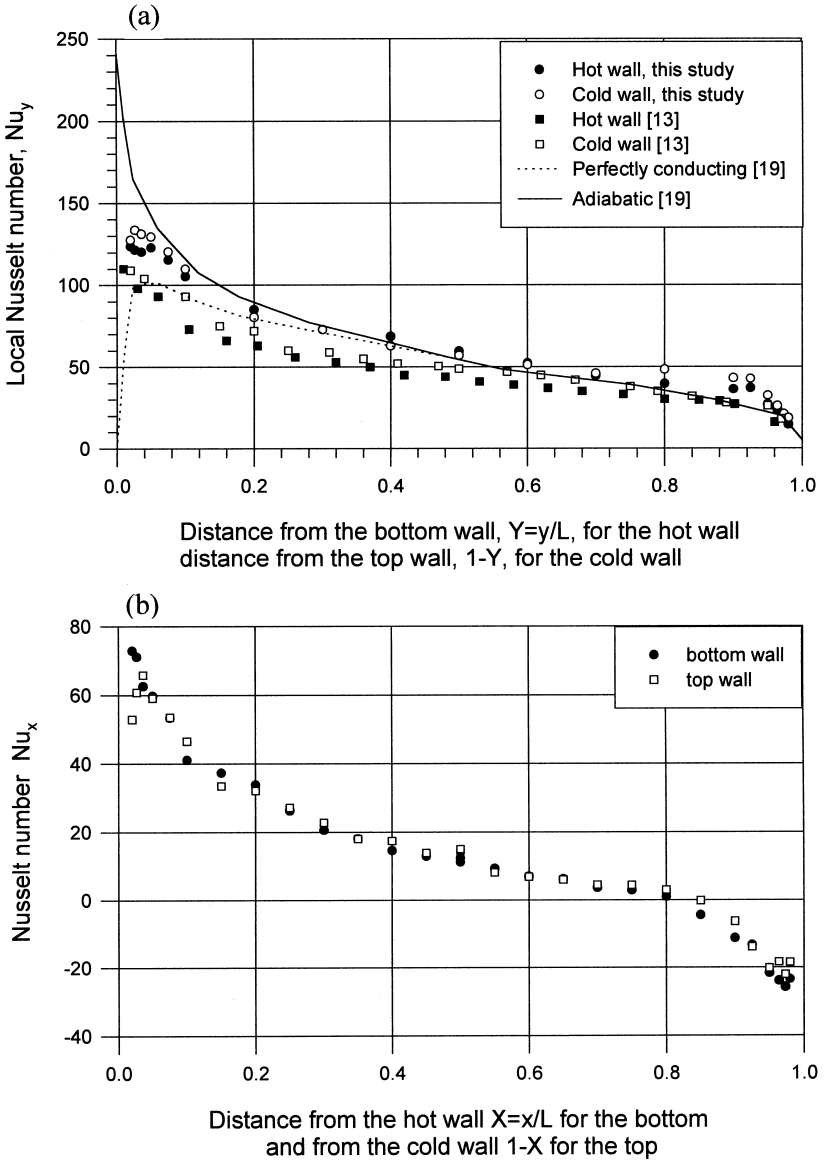

Fig. 12. Local Nu number and comparison with the experimental and numerical results at $Ra = 1.34 \times 10^9$, $Ar_x = 0.923$: (a) local Nu number along the vertical walls; (b) local Nu number along the top and bottom walls.

the wall to the air at $X = 0$–0.175 and from the air to the wall at $X = 0.175$–1. The average Nusselt number was $\overline{Nu_b} = 14.97$ (heat transfer into the cavity) and $\overline{Nu_t} = 15.67$ (heat transfer out of the cavity) for the bottom and top end walls, respectively.

Similar directly comparable past results are not available. However, it is useful to compare with some earlier work for similar conditions. Heat transfer results for an air filled cavity ($Ar_x = 0.923$ and $Ar_z = 0.288$) were experimentally reported by Mergui et al. [13] and numerically by Beghein et al. [19] at $Ra = 1.34 \times 10^9$. (Note that these authors reported their results using an Ra based on the height of the cavity, Ra_H. This can be converted to Ra by multiplying by Ar_x^3). Their results are shown in Fig. 12(a). It can be seen that Mergui et al. [13] gave lower local heat transfer rates. Although in their experiments the horizontal walls were considered adiabatic, their results are closer to the perfectly conducting wall results of Beghein et al. [19]. The numerical modelling work [12] was carried out specifically to compare with the experimental results of Mergui et al. [13]. However, it is in better agreement with the present results. The numerical modelling work indicated that at the boundary layer

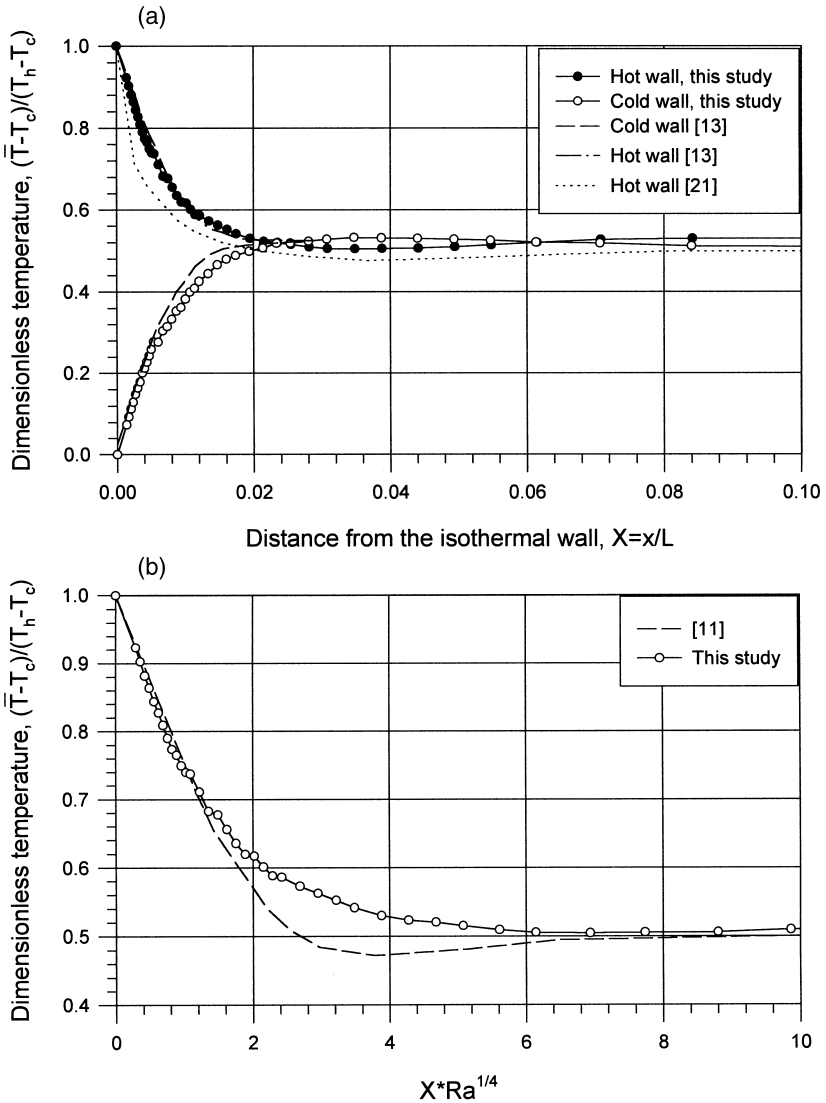

Fig. 13. Comparison of the temperature distribution near the walls at $Y = 0.5$: (a) comparison with experiments of Ref. [13] at $Ra = 1.34 \times 10^9$, $Ar_x = 0.923$ and the turbulent numerical modelling results of Ref. [21] at $Ra = 10^{10}$ and $Ar_x = 1$ with adiabatic horizontal walls; (b) comparison with laminar numerical modelling results of Ref. [10] at $Ra = 10^6$–10^{10} and $Ar_x = 1$ with adiabatic horizontal walls.

start corner (the hot-bottom and cold-top corners) the *Nu* number should be zero for a perfectly conductive horizontal wall and should be several times higher than the average value for an adiabatic horizontal wall which were not supported by the present experimental results and the results of [12] and [13]. At mid-height, the local Nusselt number was 59.5 at the hot wall and 57.1 at the cold wall. The corresponding results reported by [13] were 43.8 and 49.6. Beghein et al. [19] gave values of 54.05 and 53.82 for adiabatic and perfectly conducting horizontal walls, respectively. As mentioned above, the average *Nu* number obtained in this study was 64.0 for the hot wall and 65.3 for the cold wall. The corresponding values given by [13] were 47.6 and 53.6. The numerical results of [19] gave 63.86 and 55.59 for adiabatic and perfectly conducting horizontal walls, respectively. This means that the experimental results of [13] are lower, especially at the hot wall. The fact that they are giving different values for the hot and cold mean heat transfer rates with the hot wall value being lower, is indicative of heat exchange with the ambient or possible experimental error.

Lankhorst [11] in his numerical study gave a heat transfer correlation for laminar air flow in a square

cavity as follows:

$$Nu = 0.241 Ra^{0.260} \quad 10^6 < Ra < 10^{10} \tag{2}$$

Eq. (2) gives an Nu of 59.38 for $Ra = 1.58 \times 10^9$. Fusegi et al. [20] performed a 3D direct numerical simulation and reported that:

$$Nu = 0.163 Ra^{0.282} \tag{3}$$

which gives a Nu number of 64.0 at $Ra = 1.58 \times 10^9$. This is in perfect agreement with the present experimental results. The comparative results presented above indicate that the agreement between numerical modelling and experiments on heat transfer is good.

The mean temperature distribution at the cavity mid-height is frequently used to describe the thermal field in the cavity. The present results are compared with earlier results in Fig. 13. As shown in Fig. 13(a), the agreement between our results and the experimental results of Mergui et al. [13] is very good. They only presented results from the wall to $X = 0.028$ so no temperature over-shoot is seen in their results. The temperature distribution at the mid-height was also predicted in many numerical studies of laminar and turbulent flow. The present results are compared with the numerical laminar flow results of Lankhorst [11] and with the turbulent flow results of Beghein et al. [21]. The turbulent flow numerical results are in better agreement with the experimental results than the laminar flow numerical results. In numerical modelling involving the Boussinesq approximation, a symmetrical result is predicted so that the dimensionless temperature is 0.5 at the centre of the cavity. However, the experiments gave a slightly higher value (0.514 in this study and 0.52 in Ref. [13]). In the work of Mergui and Penot [12] and Mergui et al. [13], the temperature difference was only 20°C so that the Boussinesq approximation should be valid [22]. Further numerical modelling work can reveal the reason for the centre point temperature deviation. Although the laminar flow modelling of Lankhorst [11] predicted a thinner thermal boundary layer, the agreement near the wall is good. This means that laminar flow modelling can predict the right Nu even if as a whole, the predicted temperature field is not good enough.

In the core area, the fluid is stratified. Along the mid-width and for most part, the temperature is almost in linear distribution. The stratification parameter, Sp, given by

$$S_p = \frac{L}{T_h - T_c} \frac{\partial T}{\partial y}\bigg|_{\substack{x/L = 0.5 \\ y/L = 0.5}} \tag{4}$$

and in our case obtained by polynomial fitting, was 0.50. Ziai [15] reported a value of 0.51 and Mergui et al. [13] gave a value of 0.37. Henkes and Hoogendoorn [23] summarised contribution works to the workshop, Eurotherm Seminar 22 [24]. The stratification parameter obtained numerically ranged from 0.490 to 0.901. In the 50% range of the agreement between the numerical contributions, Sp was 0.511–0.572 and the average value was 0.539. Generally, the numerical modelling results predicated a higher value of Sp than the experimental results. The temperature distribution

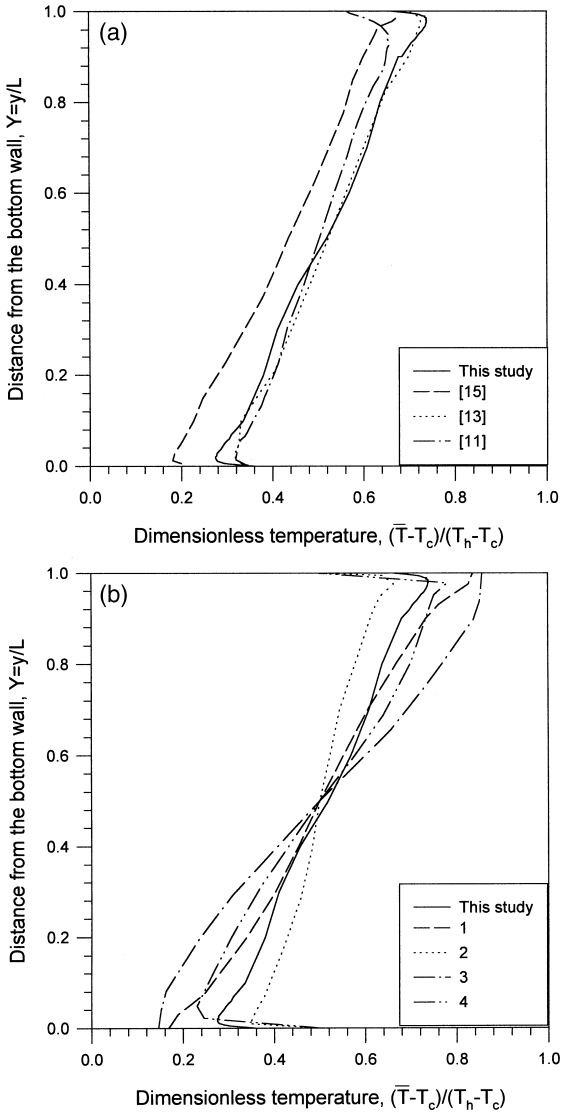

Fig. 14. Comparison of the temperature distribution along $X = 0.5$ with earlier results: (a) comparison with experimental results ([15] $Ra = 5 \times 10^8$, $Ar_x = 5$ and $Ar_z = 2$; [13] $Ra = 1.34 \times 10^9$, $Ar_x = 0.923$ and $Ar_z = 0.3$; [11] $Ra = 3.9 \times 10^8$, $Ar_x = 1$ and $Ar_z = 0.2$); (b) comparison with numerical results of [11]. (1,2 $Ra = 10^{11}$; 3,4 $Ra = 4.5 \times 10^9$; 1,3 adiabatic horizontal walls and 2,4 perfectly conducting walls).

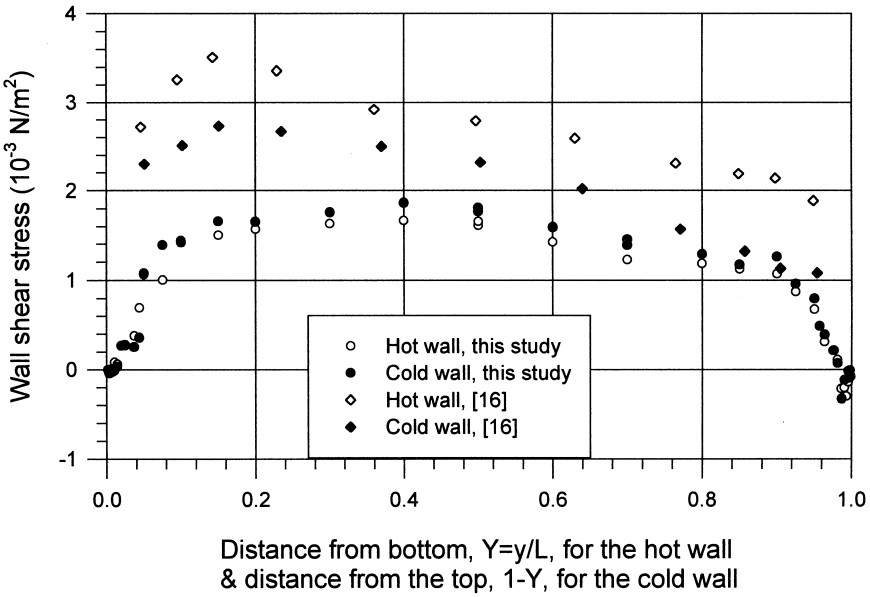

Fig. 15. Wall shear stress along the isothermal walls.

along the mid-width is compared in Fig. 14. The agreement between Mergui et al. [13] and the present results is good. The results of Ziai [15] suffered heat loss through the vertical passive wall. Lankhorst [11] made the calculation for two horizontal wall boundary conditions, i.e., adiabatic and perfectly conducting. The present results are in good agreement with the turbulent flow modelling results but different from the laminar flow modelling results. The present results (with a highly conductive horizontal wall) lie between the results obtained with the two ideal boundary conditions. Agreement is expected to improve if the real boundary condition was used in the numerical modelling.

The velocity profile in the viscous layer can be used to determine the wall shear stress. In our case, the viscous layer was about 3–4 mm thick depending on locations and the velocity profile is cubic in this layer, i.e.,

$$\bar{v} = ax + bx^2 + cx^3 \tag{5}$$

where a, b and c can vary depending on height. Then the wall shear stress can be expressed as

$$\tau_w = \mu \left.\frac{\partial \bar{v}}{\partial x}\right|_{x=0} = a \tag{6}$$

The measured results in the viscous layer were used to determine the wall shear stress by a cubic polynomial least squares fitting process. The resulting best fit equation of the velocity and location was differentiated at $X = 0$ and 1 to obtain the velocity gradient. To the best of the authors' knowledge the shear stress in a square cavity was not reported in the past. The present results are shown in Fig. 15, and agreement of the shear stress values between the two walls is good. The wall shear stress is seen not to be constant. Along the vertical walls, the boundary layer forms from the two starting corners (the bottom-hot corner and the top-cold corner). At the corner, the velocity is zero so that the wall shear stress is zero. Then, with the formation of the boundary layer, the peak velocity increased along the fluid flow direction so that the velocity gradient in the viscous layer increases. At $Y = 0.4$ ($Y = 0.6$ for the cold wall), the wall shear stress reaches its maximum. After that point, the wall shear stress decreases smoothly until the effect of the horizontal wall on the fluid becomes important. From $Y = 0.9$ ($Y = 0.1$ for the cold wall), the wall shear stress decreased sharply. The small anti-clockwise vortex at the end corner caused the wall shear stress to become negative due to the change in flow direction. The data of King [16] are also shown for comparison. His results are higher than the present ones (possibly due to a higher Ra number). The difference between the hot and cold wall results of [16] is probably due to the heat losses present in his cavity.

The experimental profile of the vertical velocity at the cavity mid-height was requested for the 1992 Eurotherm Seminar [6] to assist in the validation of numerical codes. The present data are compared with experimental and numerical results for square cavities in Fig. 16. The results of Larkhorst [11] at $Ra = 2.1 \times 10^9$ near the hot wall are in very good agreement

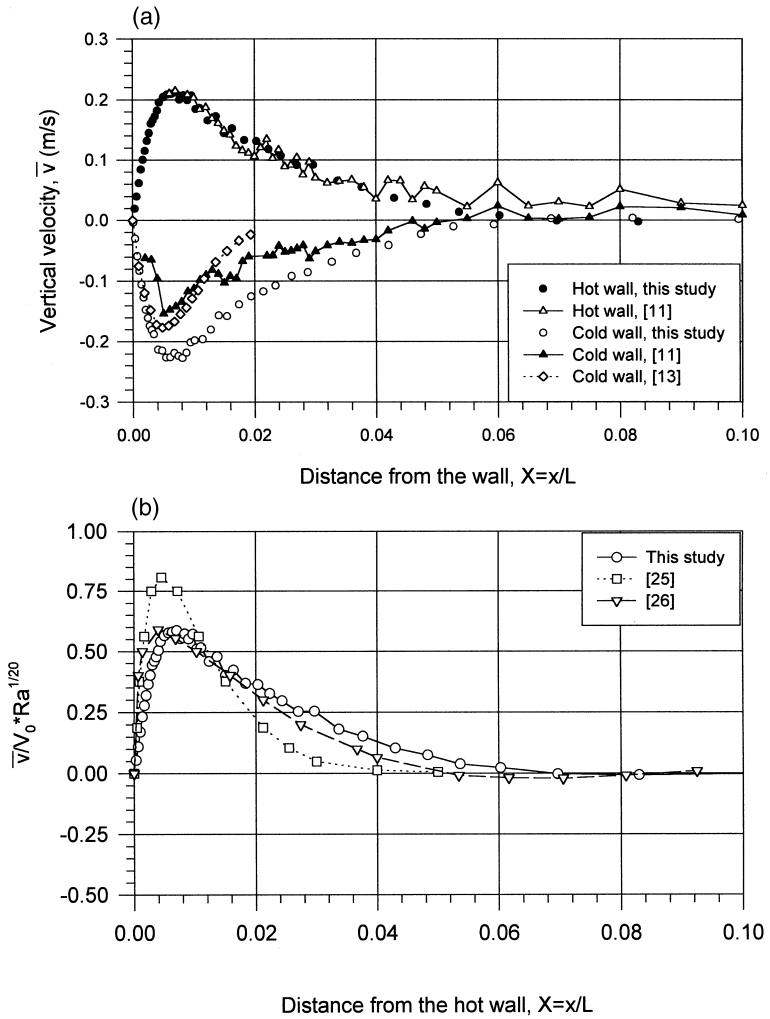

Fig. 16. Comparison of the mean vertical velocity at $Y = 0.5$: (a) experimental results (this study $Ra = 1.58 \times 10^9$; [11] $Ra = 2.1 \times 10^9$; [13] $Ra = 1.34 \times 10^9$); (b) numerical results (this study $Ra = 1.58 \times 10^9$; [25,26] $Ra = 10^{10}$).

with the present results. However, on the cold wall side, his results and the results of Mergui et al. [13] gave lower values than the present experiments. The difference between the two peak velocities in the two boundary layers (hot and cold) is quite large (28.54%) in Ref. [11], due to the small aspect ratio (only 0.1) in the depth direction ($Ar_z = 0.3$ in Ref. [13]). For these cavities, the air flow is basically three dimensional because of the influence of the heat losses through the vertical passive walls and the limited depth. In Fig. 16(b), the present results are compared with the direct simulation results of Paolucci [25]. He predicted a higher peak velocity and a thinner boundary layer. Barozzi et al. [26] gave a velocity profile at mid-height based on the k–ε model. Their results are in good agreement with our results. However, as indicated by themselves, their model tends to over-estimate the heat transfer rate. This means that near the wall a higher change rate is predicted by their model. This is seen in Fig. 16(b). They predicted a greater velocity change near the wall and a peak velocity position closer to the wall, i.e., the wall shear stress was over-estimated. Further numerical modelling with the present experimental conditions will be helpful to clarify this disagreement.

The flow parameters along the mid-height and the mid-width are both important in the description of the flow features in the cavity. However, parameters along the mid-width have not received as much attention as the parameters along the mid-height, specially in experimental works. The results obtained in this study are shown in Fig. 17. Experimental measurements confirm that the air in the cavity is stationary between $Y = 0.25$ and 0.75. Flow reversal exists along the outer

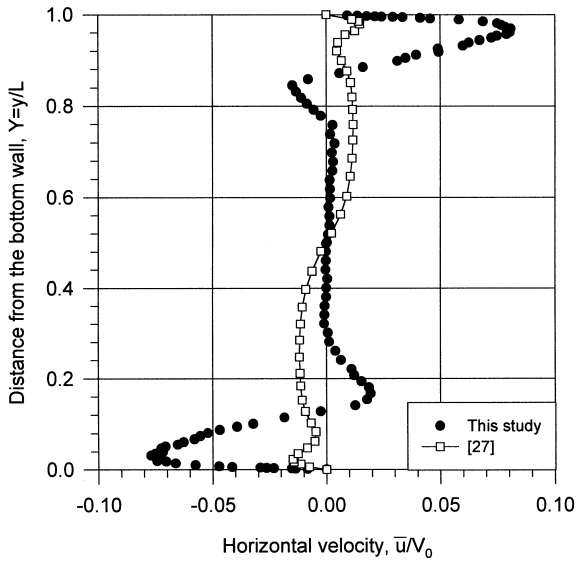

Fig. 17. Comparison of the mean horizontal velocity at mid-width (this study $Ra = 1.58 \times 10^9$; [27] $Ra = 10^{10}$, $Ar_x = 1$).

edge of the horizontal boundary layer. The numerical modelling results of Beghein et al. [27] indicated that the air is moving everywhere except at the centre of the cavity and no flow reversal was found. This means that in this numerical modelling work only the flow near the active walls is correctly described. Further numerical modelling with the present experimental conditions will eliminate boundary condition effects and will be helpful in fully understanding the basic structure of the whole turbulent air flow in the cavity. The turbulence quantities and their detailed analysis are given in Part II of this work [7].

5. Conclusions

An experimental investigation of low turbulence natural convection in an air filled square cavity was conducted at $Ra = 1.58 \times 10^9$. The cavity, with an aspect ratio of 2 in the depth direction and two guard cavities, offered two dimensional flow at the cavity middle plane. At this Ra number, low level turbulent flow exists in the cavity. The flow is limited in a narrow strip along the walls where the velocity and temperature change sharply. In the vertical boundary layer, the velocity reached its maximum value between the buoyant sub-layer and the outer layer and decreased to negative values at the outer edge of the boundary. The negative values are the result of four vortices — one on each wall lying outside the boundary layer flow. Two additional, much smaller vortices, were obtained at the hot top and cold bottom corners. The fluid in the cavity core ($X = 0.1$–0.9, $Y = 0.25$–0.75) was stationary and stratified. The wall shear stress was obtained from the measured velocity in the viscous layer. Similar distributions and values were obtained for both the hot and the cold walls. The temperature distribution in the cavity was nearly anti-symmetrical about the cavity centre. The temperature distribution was used to record the thermal conductive layer which was found to be approximately 3 mm at the mid-height. The local Nu was again anti-symmetrical and the agreement between the average value at the hot and cold walls was excellent. Compared with earlier results, the agreement on the Nu is good. Acceptable agreement was also found when comparing the temperature and velocity profiles at mid-height. Differences were found along the mid-width and the change rates near the walls. The results described in this paper were obtained with high precision and can be useful as benchmark data for comparison with CFD codes. Such numerical simulation should include realistic boundary conditions at the top and bottom horizontal walls as given in this study.

References

[1] I. Catton, Natural convection in enclosures, in: Proc. Sixth Int. Heat Transfer Conf., vol. 2, Toronto, Canada, 1978, pp. 13–20.
[2] C.J. Hoogendoorn, Natural convection in enclosures, in: Proc. Eighth Int. Heat Transfer Conf., vol. 1, San Francisco, USA, 1986, pp. 111–120.
[3] S. Ostrach, Natural convection in enclosures, Trans. of ASME, J. Heat Transfer 110 (1988) 1175–1190.
[4] K.T. Yang, Natural convection in enclosures, in: S. Kakac, R.K. Shah, W. Aung (Eds.), Handbook of Single-Phase Convective Heat Transfer, Wiley, New York, 1987 (Chapter 13).
[5] K.T. Yang, Transitions and bifurcations in laminar buoyant flows in confined enclosures, Trans. ASME, Journal of Heat Transfer 110 (1988) 1191–1204.
[6] R.A.W.M. Henkes, C.J. Hoogendoorn (Eds.), Turbulent Natural Convection in Enclosures — A Computational and Experimental Benchmark Study, Editions Europeennes Thermique et Industrie, 1993.
[7] Y.S. Tian, T.G. Karayiannis, Low turbulence natural convection in an air filled square cavity Part II: the turbulence quantities, Int. J. of Heat Mass Transfer 43 (2000) 867–884.
[8] Y.S. Tian, Low turbulence natural convection in an air filled square cavity, Ph.D. thesis, South Bank University, London, UK, 1997.
[9] F. Allard, Effects of thermal boundary conditions on natural convection in thermally-driven cavities, in: R.A.W.M. Henkes, C.J. Hoogendoorn (Eds.), Turbulent Natural Convection in Enclosures — A Computational and Experimental Benchmark Study, Editions Europeennes Thermique et Industrie, 1993, pp. 214–233.
[10] F. Penot, A. N'Dame, Successive bifurcations of natural

convection in a vertical enclosure heated from the side, in: Heat Transfer, Third UK National Conference and First European Conference on Thermal Sciences, vol. I, Birmingham, UK, 1992, pp. 507–513.

[11] A.M. Lankhorst, Laminar and turbulent natural convection in cavities — numerical modelling and experimental validation, Ph.D. thesis, Technology University of Delft, The Netherlands, 1991.

[12] S. Mergui, F. Penot, Natural convection in a differentially heated square cavity — experimental investigation at $Ra = 1.69 \times 10^9$, Int. J. Heat Mass Transfer 39 (1996) 563–574.

[13] S. Mergui, F. Penot, J.L. Tuhault, Experimental natural convection in an air-filled square cavity at $Ra = 1.7 \times 10^9$, in: R.A.W.M. Henkes, C.J. Hoogendoorn (Eds.), Turbulent Natural Convection in Enclosures — A Computational and Experimental Benchmark Study, Editions Europeennes Thermique et Industrie, 1993, pp. 97–108.

[14] I.J. Opstelten, C.M. Zhang, H.S. Dol, C.J. Hoogendoorn, Turbulent quantities of a natural convection flow in a side-heated enclosure; experiments and calculations, in: Proc of Second European Thermal-Sciences and Fourteenth UIT National Heat Transfer Conference, 1996, pp. 795–802.

[15] S. Ziai, Turbulent natural convection in a large rectangular air cavity, Ph.D. thesis, Queen Mary and Westfield College, University of London, London, UK, 1983.

[16] K.J. King, Turbulent natural convection in rectangular air cavities, Ph.D. thesis, Queen Mary and Westfield College, University of London, London, UK, 1989.

[17] W.K. George, S.P. Capp, A theory for natural convection turbulent boundary layer next to heated vertical surfaces, Int. J. Heat Mass Transfer 22 (1979) 813–826.

[18] J.T. Davies, Turbulence Phenomena, Academic Press, New York, 1972.

[19] C. Beghein, F. Penot, S. Mergui, F. Allard, Numerical and experimental evaluation of turbulent models for natural convection simulation in a thermally driven square cavity, in: Proc. of the ASME Conf., 93-WA/HT-46, 1993, pp. 1–12.

[20] T. Fusegi, J.M. Hyun, K. Kuwahara, Three-dimensional simulations of natural convection in sidewall-heated cube, Int. J. for Numerical Methods 13 (1991) 857–867.

[21] C. Beghein, F. Allard, A. Draoui, Numerical modelling of turbulent convection in a thermally-driven square cavity, R.A.W.M. Henkes, C.J. Hoogendoorn (Eds.), Turbulent Natural Convection in Enclosures — A Computational and Experimental Benchmark Study, Editions Europeennes Thermique et Industrie, 1993, pp. 31-42.

[22] D.D. Gray, A. Giorgini, The validity of the Boussinesq approximation for liquids and gases, Int. J. Heat Mass Transfer 19 (1976) 545–551.

[23] R.A.W.M. Henkes, C.J. Hoogendoorn, Comparison of the standard case for turbulent natural convection in a square enclosure, in: R.A.W.M. Henkes, C.J. Hoogendoorn (Eds.), Turbulent Natural Convection in Enclosures — A Computational and Experimental Benchmark Study, Editions Europeennes Thermique et Industrie, 1993, pp. 185–213.

[24] R.A.W.M. Henkes, C.J. Hoogendoorn, Turbulent natural convection in enclosures, in: R.A.W.M. Henkes, C.J. Hoogendoorn (Eds.), Turbulent Natural Convection in Enclosures — A Computational and Experimental Benchmark Study, Editions Europeennes Thermique et Industrie, 1993, pp. 64–75.

[25] S. Paolucci, Direct numerical simulation of two-dimensional turbulent natural convection in an enclosed cavity, J. Fluid Mech 215 (1990) 229–262.

[26] G.S. Barozzi, E. Nobile, A.C.M. Sousa, Contribution to the numerical simulation of turbulent natural convection in rectangular enclosures, in: R.A.W.M. Henkes, C.J. Hoogendoorn (Eds.), Turbulent Natural Convection in Enclosures — A Computational and Experimental Benchmark Study, Editions Europeennes Thermique et Industrie, 1993, pp. 19–30.

[27] C. Beghein, F. Allard, A. Draoui, Numerical modelling of turbulent convection in a thermally-driven square cavity, in: R.A.W.M. Henkes, C.J. Hoogendoorn (Eds.), Turbulent Natural Convection in Enclosures — A Computational and Experimental Benchmark Study, Editions Europeennes Thermique et Industrie, 1993, pp. 31–42.